ADVANCED OPTICAL MATERIALS
www.advopticalmat.de

Resonant Plasmon-Enhanced Absorption of Charge Transfer Complexes in a Metal–Organic Monolayer

Denis M. Krichevsky, Alexander Yu. Tolbin, Tatiana V. Dubinina, Sergey S. Kosolobov, Vitally I. Krasovskii, Larisa G. Tomilova, Victor E. Pushkarev, and Anton V. Zasedatelev**

Plasmonic enhancement of absorption in charge-transfer (CT) complexes formed under NO_2 gas adsorption onto 2D hybrid structure, based on the metal–organic monolayer and gold nanoparticles (AuNPs), is demonstrated. By using Langmuir–Blodgett deposition of low-symmetry zinc phthalocyanine (ZnPc) molecules, the metal–organic monolayer is fabricated with greatly suppressed intermolecular aggregation. Oxidation of the monolayer through coordination of NO_2 molecules with axial zinc ions of ZnPc molecules gives rise to the specific absorption band inherited to cation radical $ZnPc^+$. The hybrid AuNPs–ZnPc structure is engineered to maximize exciton–plasmon interaction of CT complexes at the radical form of the metal–organic monolayer. Excellent spectral and spatial overlaps with plasmon resonance boost absorption of CT internal optical transition, so-called "fingerprint" band, by a factor of six from 0.45% to 2.8% in total. The approach paves the way for efficient plasmonic control over photochemical reactions promoted by charge-transfer complexes in metal–organic films. In particular, the plasmonic effect is harnessed to improve NO_2 gas sensing properties; the experimental study shows a 15-fold increase of the detection efficiency in the specific band of CT complexes under the gas exposure.

1. Introduction

Owing to their unique physical and chemical properties, 2D organic materials with large π-conjugated electronic system have recently emerged as the promising building block for different applications. Among the huge class of metal–organic compounds, phthalocyanines attract much attention in science since their first synthesis in 1907[1] to nowadays and are widely used in the industry as pigments and drugs for photodynamic treatment of cancer.[2] Phthalocyanines constitute a very rich family of compounds enabling coordination with more than 70 elements of the periodic table in their central coordination site alongside with numerous possible substituents at the periphery. Possessing an 18 π-electron conjugation system in their neutral redox state, phthalocyanines demonstrate remarkable optical properties which are extensively studied for potential applications in organic and hybrid photovoltaics (PV), optical memory devices,[3] photodynamic therapy (PDT), and fluorescence diagnostics of cancer,[4] optical gas sensors,[5,6] and field-effect transistors,[7,8] photocatalysis,[9,10] and light-harvesting elements in artificial photosynthetic systems.[11,12] At the same time, radical forms of phthalocyanines are of great interest for organic magnetism and molecular spintronics.[13] In this respect, phthalocyanine

D. M. Krichevsky
Moscow Institute of Physics and Technology
National Research University
9, Institutskiy per., Dolgoprudny, Moscow 141701, Russia
E-mail: kirchevskii.dm@phystech.edu

D. M. Krichevsky
Russian Quantum Center
30, street Bolshoy Bulvar, building 1, Skolkovo Innovative Center,
Moscow 143026, Russia

Prof. A. Y. Tolbin, Dr. T. V. Dubinina, Prof. L. G. Tomilova,[†]
Dr. V. E. Pushkarev
Institute of Physiologically Active Compounds
Russian Academy of Sciences
1, Severnyproezd, Chernogolovka, Moscow Region 142432, Russia

The ORCID identification number(s) for the author(s) of this article can be found under https://doi.org/10.1002/adom.202100065.

Dr. T. V. Dubinina, Prof. L. G. Tomilova[†]
Department of Chemistry
Lomonosov Moscow State University
1, Leninskie Gory, Moscow 119991, Russia

Dr. S. S. Kosolobov, Dr. A. V. Zasedatelev
Skolkovo Institute of Science and Technology
3, Nobel street, Moscow 143026, Russian
E-mail: a.zasedatelev@soton.ac.uk

Dr. V. I. Krasovskii
A. M. Prokhorov General Physics Institute
Russian Academy of Sciences
38, Vavilov Street, Moscow 119991, Russian

Dr. A. V. Zasedatelev
Department of Physics and Astronomy
University of Southampton
Southampton SO17 1BJ, United Kingdom

[†]Prof. Larisa G. Tomilova passed away on the 4th of January, 2021.

DOI: 10.1002/adom.202100065

monolayers in their radical forms can be utilised for building 2D arrays of single-molecule magnets.[13–16]

Besides the aforementioned traditional applications of phthalocyanine compounds, there are new fields recently emerged with a promise for advanced optoelectronic devices based on principles of strong light-matter interaction[17,18] and topological physics.[19] It is worth noting very recent reports on the substantial improvement in performances of optoelectronic devices based on interfaced monolayers of transition-metal dichalcogenides (TMDC) and metal-phthalocyanines. Such 2D inorganic–organic semiconductor heterostructures were shown to favor effective charge separation following exciton formation under optical excitation of TMDC monolayer or phthalocyanine molecules depending on the interplay between energy levels.[20–23] In particular, zinc phthalocyanine molecules being coupled to atomically thin MoS_2 exhibit type-II band alignment at the interface allowing for ultrafast electron transfer from zinc phthalocyanine to MoS_2[23] while the reverse charge transfer is possible if it couples to WSe_2 with the higher-lying conductance band.[21]

Monolayers of metal phthalocyanines offer the unique material platform for many fascinating applications, but its low optical density severely limits their potential. The coupling of phthalocyanines with metal nanostructures exhibiting strong plasmonic resonance is a well proven strategy to clear the hurdle. In our previous work, we showed significant increase and spectral extension of light absorption in phthalocyanine molecules adjacent to gold particles.[24] Such hybrid systems based on metal-phthalocyanines and gold nanoparticles are very attractive objects as they encompass unique constellation of plasmonic and excitonic properties alongside with rich photochemistry of metal–organics. Being a promising model platform to study plethora of plasmon-assisted phenomena, this type of nanostructures have already demonstrated significant increase in the quantum yield of singlet oxygen generation,[25–27] cytotoxic agent for photodynamic therapy (PDT) of cancer cells, and highly reacting agent triggering variety of chemical reactions.[28] One may anticipate a range of plasmon-enhanced photoinduced processes out of such hybrid systems, namely nonlinear optical response,[29–33] photocurrent generation,[33–35] fluorescence,[36–38] SERS,[39,40] and other related phenomena.

In this study, we have designed and fabricated 2D hybrid structure based on the low-symmetry zinc phthalocyanine (ZnPc) monolayer and gold nanoparticles (AuNPs) using simple and scalable Langmuir–Blodgett deposition method. We study optical absorption of ZnPc monolayer in its neutral and cation radical forms following coordination with NO_2 molecules under the gas exposure. Our in-depth analysis reveals plasmonic effects promoting light absorption of specific internal optical transition, also known as a "fingerprint" band, which in turn significantly modifies absorption spectrum of the monolayer in the radical form. We scrutinize NO_2 detection response at the mixed exciton–plasmon absorption band and quantify the impact of the main contributions.

2. Results and Discussion

To form the densely packed monolayer of gold nanoparticles, we implement in situ control of both: its surface pressure and absorption spectra. **Figure 1**a shows pressure-area isotherm of AuNPs monolayer on the subphase, where the transition from so-called gaseous phase of the Langmuir monolayer to the solid one appears when subphase area (SA) reaches 275 cm^2. With further squeezing barriers, we observe a collapse of the monolayer at the surface pressure of ≈17 mN/m (SA ≈ 225 cm^2) which is consistent with previous studies.[47,48] Similarly, we identify the collapse point from absorption spectra of the Langmuir AuNPs monolayer measured in situ at different subphase area and pressure as shown in Figure 1b The absorption band centered at ≈530 nm corresponds to localized surface plasmon (LSP) resonance in gold nanoparticles. Our spectral analysis indicates linear dependence of optical density on the SA above 190 cm^2. Figure 1c shows the spectral maxima as the function of area demonstrating a similar trend within the region >190 cm^2. However, the monolayer breaks down to inhomogeneous multilayer structure followed by changing the slope below this value. It is worth noting that LSP resonance peak position of the AuNP Langmuir monolayer undergoes spectral redshift during compression which is the consequence of decreasing the interparticle distance. Unlike the magnitude of absorption and LSP resonance peak position, the form of spectra remains the same regardless of the area (Figure 1b). Thus, we define surface pressure of 15 mN m^{-1} is optimal to transfer densely packed AuNPs monolayer onto the substrate. In order to decrease the influence of the thiol shell on the interaction with ZnPc molecules, we anneal the monolayer film of AuNPs at 230 °C during 1 h as shown schematically in Figure 1d The sintering of the film results in desorption of thiol shells followed by agglomeration to larger particles that can be witnessed through the LSP-band narrowing in Figure 1e and via direct analysis of scanning electron microscopy (SEM) image of the AuNPs monolayer structure (Figure 1f). Histograms in Figure 1g,h demonstrate interparticle first neighbor distance and particle size distributions in the sintered AuNPs monolayer structure, respectively. According to statistical analysis of the SEM image, the average interparticle distance and particle diameter are of 18.6 nm (standard deviation $\sigma = 7.12$ nm) and 5.7 nm (standard deviation $\sigma = 3.62$ nm), respectively. A cross-section of the AuNPs SEM image is presented in Section S2b, Supporting Information.

The low-symmetry zinc phthalocyanine complex used in the study does not exhibit distinct transition from gas to the liquid phase in terms of pressure-area isotherm of the Langmuir ZnPc monolayer. However, **Figure 2**a shows 2D solid phase appearing below 160 cm^2 alongside the change in optical density of the Langmuir ZnPc monolayer. In turn, the optimal surface pressure to transfer ZnPc monolayer is defined at 30 mN m^{-1}. We transfer the Langmuir ZnPc monolayer on top of the AuNPs monolayer structure and on the bare glass substrate as the reference for further analysis. Figure 2b shows absorption spectra of both AuNPs-ZnPc and glass-ZnPc monolayer structures. The bare glass-ZnPc monolayer exhibits the main peak at 685 nm originated from the Q-band of ZnPc monomers and the secondary maximum at 620 nm which is related to the small fraction of H-type aggregates, inevitably present in the amount of ≈10%. In contrast to glass-ZnPc, AuNPs–ZnPc monolayer structure exhibits two well-defined maxima at ≈530 and ≈685 nm attributed with LSP-band and Q-band absorption, respectively.

It is worth noting significant spectral detuning between the Q-band of ZnPc and LSP-band of gold nanoparticles in the AuNPs–ZnPc monolayer structure. Therefore, it is very unlikely the system is capable to support strong exciton–plasmon

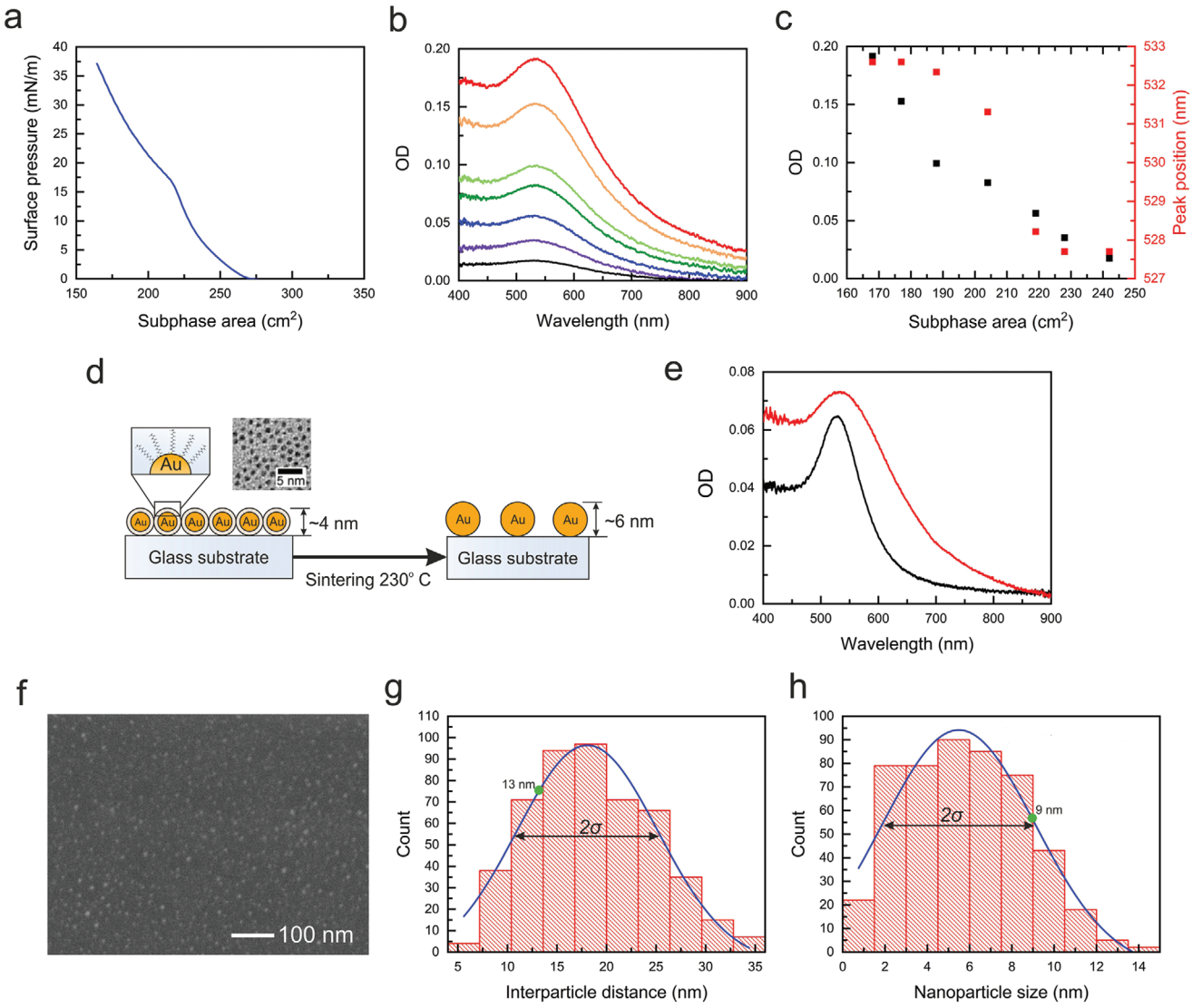

Figure 1. Formation of the AuNPs monolayer. a) Pressure–area isotherm of the Langmuir AuNPs monolayer. b) Absorption spectra of the Langmuir AuNPs monolayer recorded in situ during compression (black – 5 mN m^{-1} (242 cm^2), purple – 10 mN m^{-1} (228 cm^2), blue – 15 mN m^{-1} (219 cm^2), dark green – 20 mN m^{-1} (204 cm^2), light green – 25 mN m^{-1} (188 cm^2), orange – 30 mN m^{-1} (177 cm^2), red – 35 mN m^{-1} (168 cm^2)). c) Optical density and spectral position of absorption peak of the Langmuir AuNPs monolayer as a function of subphase area. d) Scheme of the AuNPs monolayer deposited on a glass substrate before and after sintering process. e) Absorption spectra of the AuNPs monolayer deposited on a glass substrate before (red) and after (black) sintering (red). f) SEM image of the sintered AuNPs monolayer. g,h) Statistical histograms of the interparticle first neighbor distance and particles diameter in the sintered AuNPs monolayer structure, respectively. Green dots are the best-fit results of interparticle distance (a) and nanoparticle size (b) used in FDTD simulations.

interaction regime in its neutral form. Indeed, resonant frequencies of both exciton and plasmon bands change slightly upon interaction. In **Figure 3**a, we compare the experimental absorption spectra of hybrid AuNPs–ZnPc structure with the bare AuNPs and ZnPc monolayers and their superposition. There is a measurable increase in absorption of exciton and plasmon bands across the whole spectrum range from 500 to 700 nm. To shed light on the mechanisms of the spectral features observed, we performed FDTD numerical simulations of the absorption spectra. Figure 3b demonstrates results of simulations, where the uniformly-distributed 9 nm gold nanoparticles with the period of 13 nm and 2.5 nm ZnPc monolayer on a SiO_2 substrate have been employed to model bare AuNPs and ZnPc monolayer structures, respectively. These parameters correspond to the best-fit result. A deviation from maxima of the distributions in Figure 1g,h reflects a slight non-uniformity of the sample. The thickness of the ZnPc monolayer of 2.5 nm was defined experimentally from atomic force microscopy (AFM) study of the bare ZnPc monolayer on a glass substrate (see Figure S2, Supporting Information). To model the hybrid AuNPs–ZnPc structure, we combine both monolayers together on the single SiO_2 substrate according to schematic in Figure 3b. Our numerical simulations meet a remarkable agreement with the experimental spectra. Indeed, considering the bare monolayers, one can see the exact match with experimental data in the exciton Q-band absorption of ZnPc molecules located at 685 nm and quantitative agreement in the LSP-band of AuNPs with the optical density of 0.068 at

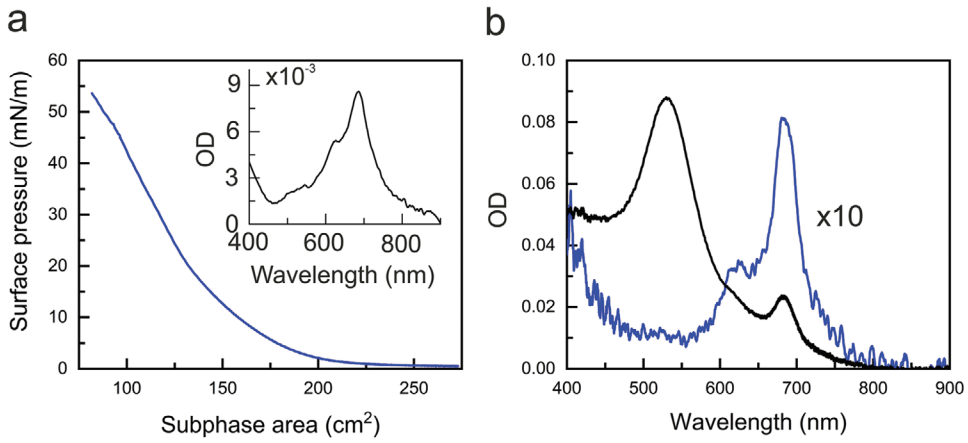

Figure 2. ZnPc deposition on a glass substrate and on top of the AuNPs monolayer. a) Isotherm graph of ZnPc on water subphase (inset – absorption spectrum reordered in situ at 30 mN m^{-1}). b) Absorption spectra of the hybrid AuNPs–ZnPc structure (black) and the bare ZnPc monolayer on a glass substrate multiplied by 10 (blue).

517 nm. The only discrepancy between experimental data and model results is visible in the width of LSP resonance, which is slightly narrowed in our simulations. Apparently, the effect comes from a dispersion in the particle size and interparticle distance shown in Figure 1e,f Note, our model does not take it into account, but deals with the mean values instead.

We would like to highlight an importance of the simulation for understanding non-additive spectral features of the hybrid AuNPs–ZnPc structure. Within the picture of weak exciton-plasmon interaction, there are two primary effects behind the increase of optical density: plasmonic enhancement of absorption in ZnPc molecules nearby gold nanoparticles[24] and LSP resonance amplification due to the high refractive index of surrounding ZnPc monolayer. To discriminate between these contributions and extract pure enhancement factor of ZnPc absorption in the hybrid structure, we calculate *E*-field distribution acting on the molecules and integrate over the whole ZnPc layer. As the result, we get a spectrum of the integrated intensity $|E|^2$ enhancement demonstrating up to sixfold increase in the peak of LSP resonance and almost three times enhancement at the maximum of excitonic Q-band transition shown in **Figure 4**a. The near field acts on the ZnPc molecules thus shaping their effective absorption spectrum. Figure 4b shows ZnPc absorption in the hybrid and bare monolayer structures. By subtracting the part absorbed in the ZnPc monolayer from the spectrum of the hybrid structure as a whole, we extract the amplification factor of the LSP resonance equals 1.5 times. The quantitative analysis of both contributions is given in Section S8, Supporting Information.

Importantly, the spectral absorption patterns of the AuNPs–ZnPc hybrid structure and the sum of its components are in excellent agreement indicating that the mechanism of spectral changes in the hybrid system is most likely of a purely electromagnetic nature without the contribution of chemical and/or photochemical effects. In contrast, the interaction of ZnPc with nitrogen dioxide exhibits a redox character: a charge-transfer (CT) complex $[ZnPc]^{+\bullet}$–$[NO_2]^-$ is formed, in which ZnPc is present in its one-electron oxidized cation-radical form.[49–51] This CT complex is presumably formed during the coordination of the NO_2 molecule at the zinc atom in ZnPc.[52–55] The transition of ZnPc to $[ZnPc]^{+\bullet}$ in the complex with nitrogen dioxide

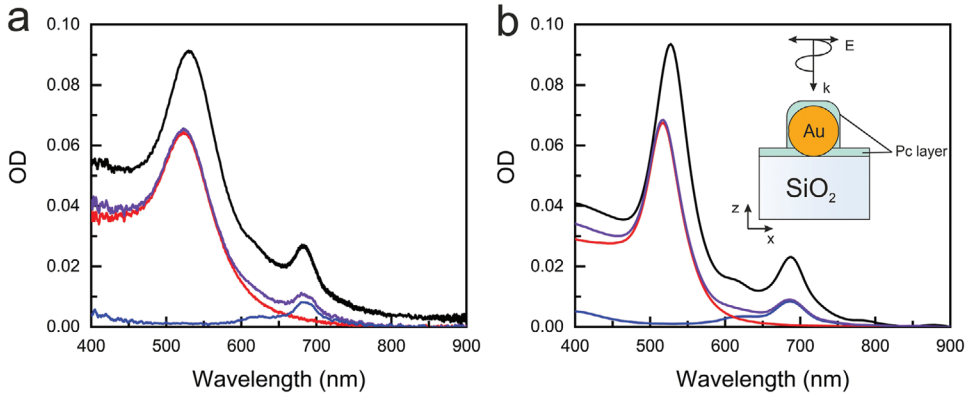

Figure 3. Understanding the spectral features. a) Absorption spectra of the hybrid AuNPs–ZnPc structure (black), the bare ZnPc (blue), and AuNPs (red) monolayer, and the sum of the bare monolayers (purple). b) Numerical simulations of absorption spectra of the hybrid AuNPs–ZnPc structure (black), the bare ZnPc (blue), and AuNPs (red) monolayer, and the sum of the bare monolayers (purple) (inset – scheme of the unit cell of the simulated structure).

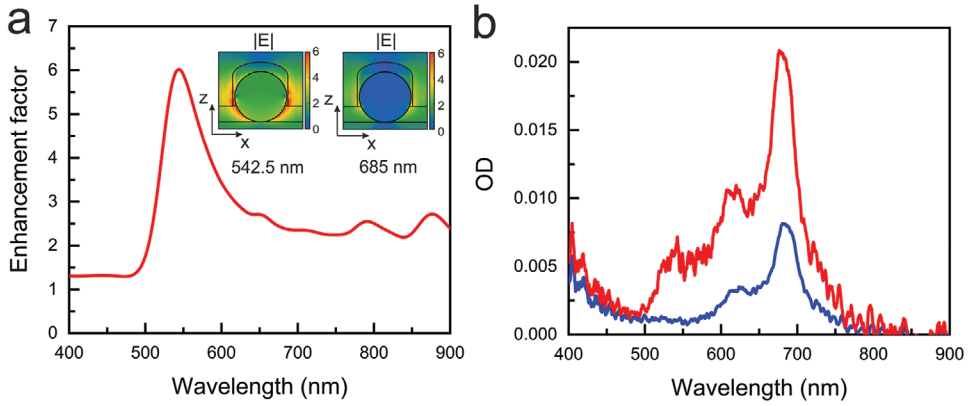

Figure 4. Effective absorption spectrum of ZnPc monolayer in the hybrid structure. a) Absorption enhancement factor of ZnPc molecules in the hybrid AuNPs structure as a function of wavelength. Inset – spatial distribution of E-field /*E*/ in the hybrid structure, black lines represent contours of AuNP and ZnPc layers. b) Effective spectra of ZnPc monolayer in the hybrid structure (red) and absorption spectrum of the bare ZnPc monolayer (blue).

leads to the quenching of the initial Q-band absorption and the appearance of the so-called "fingerprint" band in the region of ≈520 nm (see Figure S5, Supporting Information), associated with the single-electron excitations from low-lying doubly occupied orbitals $5e_g$, $6e_g$ (HOMO–*n*) toward the half-empty $2a_{1u}$ orbital (SOMO).[49] We also managed to observe the appearance of this band under the action of NO_2 on a bare monolayer of the ZnPc studied herein (**Figure 5**a). Our quantum-chemical calculations based on density-functional theory (DFT) confirm the origin of the band appeared at ≈520 nm and assign it to the internal optical transition being the hallmark of the CT-complex formation. Figure 5b indicates simplified energy level diagram and configurations of molecular orbitals related to the dominant optical transitions of $[ZnPc]^{+\bullet}$–$[NO_2]^-$ CT complex. Notably, the CT-complex formation process is reversible (see Sections S5 and S6, Supporting Information). Desorption of NO_2 can be achieved by a gentle heating (60 °C) without affecting intermolecular arrangement of the monolayer.[44]

There is one unique feature that we exploited engineering our hybrid structure – the frequency of the "fingerprint" band perfectly matches LSP resonance frequency. In a few lines below, we provide details regarding essential role of the spectral overlap in plasmon-enhanced NO_2 detection. **Figure 6**a shows the response of the hybrid AuNPs–ZnPc structure to NO_2 exposure (300s) under the same conditions utilised for the bare ZnPc monolayer in Figure 5a We observe almost complete quenching of the Q-band absorption at 685 nm and significant change at LSP-band accompanied with 13 nm red shift of its resonance. To compare the response of the bare ZnPc monolayer with its hybrid exciton–plasmon counterpart, we plot differential spectra Δ*A* calculated as the absorption difference of the structure before and after NO_2 exposure (300s), Figure 6b shows the result. We observe increase of the response by a factor of 3.5 at the Q-band absorption and 15-fold increase at the coupled "fingerprint"-LSP band. It is worth to mention the absorption change depends on the exposure time, for details see Section S7, Supporting Information. To gain more insight into origins of the large enhancement at this specific band, we have simulated the spectra using modified complex permittivity of $ZnPc^+$-NO_2^- layer which we derived from experimental data by means of Kramers–Kronig analysis using absorption spectrum of the bare ZnPc monolayer under NO_2 exposure (for details see

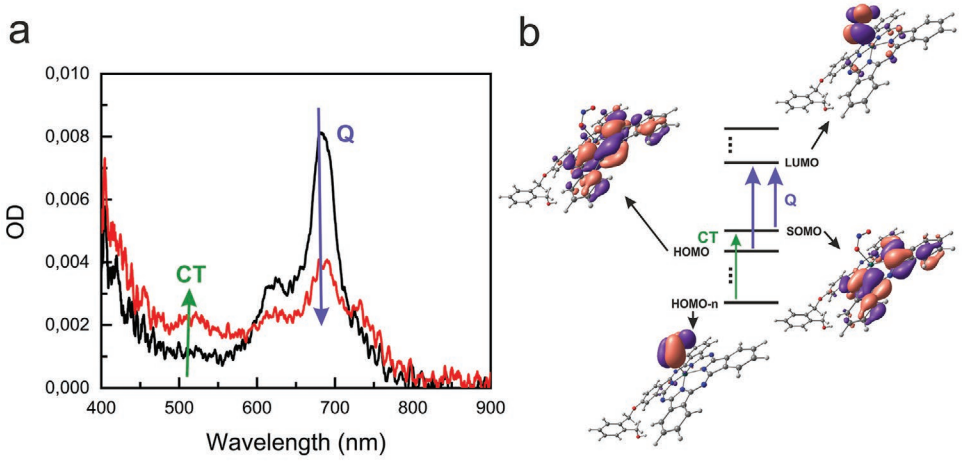

Figure 5. Photochemistry of ZnPc–NO_2 interaction. a) Absorption spectra of the bare ZnPc monolayer before (black) and after (red) 300s NO_2 exposure. Green and blue arrows indicate increase of CT and quenching of Q-band absorption, respectively. b) Energy diagram and configurations of HOMO–*n*, HOMO, SOMO, and LUMO molecular orbitals, and corresponding transitions calculated using density-functional theory (DFT).

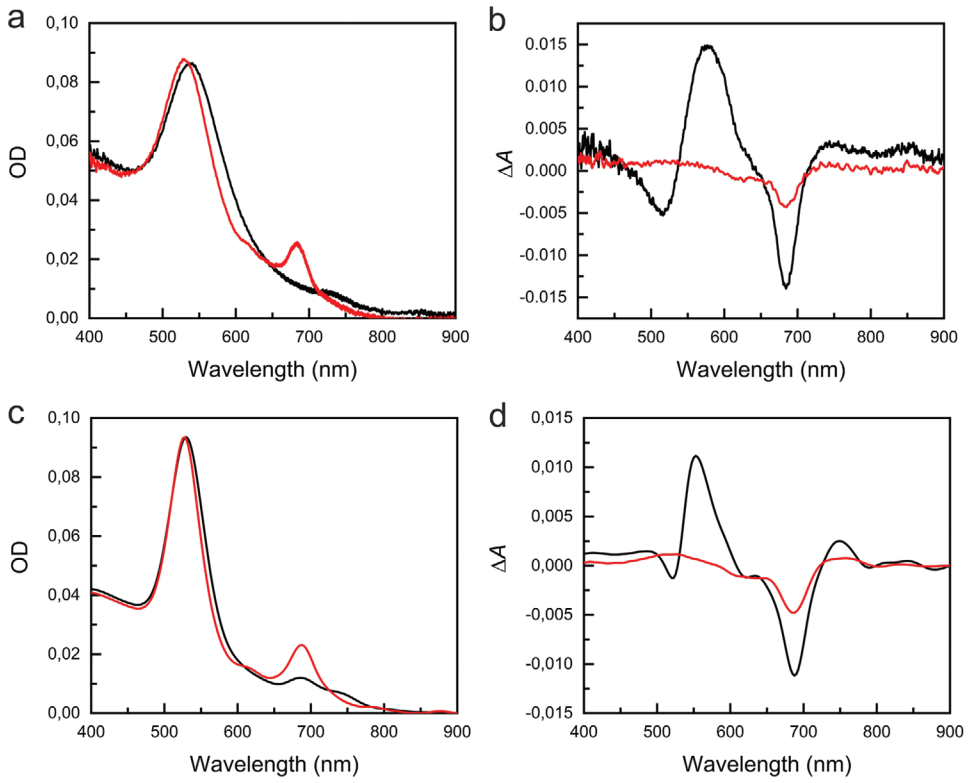

Figure 6. Plasmonic enhancement of NO_2 detection. a) Absorption spectra of the hybrid AuNPs–ZnPc monolayer before (red) and after (black) 300s NO_2 exposure. b) Differential absorption spectra ΔA of the bare ZnPc monolayer (red) and the hybrid AuNPs–ZnPc structure (black). c) Numerical simulations of absorption spectra of the hybrid AuNPs–ZnPc structure before (red) and after (black) NO_2 exposure. d) Numerical simulations of differential absorption spectra ΔA of the bare ZnPc monolayer (red) and the hybrid AuNPs–ZnPc structure (black).

Optical constants of the bare ZnPc monolayer", in Supporting Information). Figure 6c,d reveals excellent agreement of model results with experimental data. Notably, we observe the differential spectrum of the hybrid structure under NO_2 exposure exhibits the same antisymmetric s-shaped resonance with negative and positive extrema at 510 and 580 nm, respectively.

We consider two reasons giving rise for the asymmetric resonance at the coupled "fingerprint"-LSP band, namely plasmon-assisted light absorption of CT complexes via the HOMO–n → LUMO optical transitions and a redshift of LSP resonance upon altering dielectric function of the surrounding.[56] According to the E-field calculation depicted in Figure 4a, we anticipate strong absorption enhancement in the "fingerprint" band; however, one should take into account modified permittivity of the ZnPc layer under NO_2 exposure. In **Figure 7**a, we superimpose integrated spectra of intensity $|E|^2$ enhancement

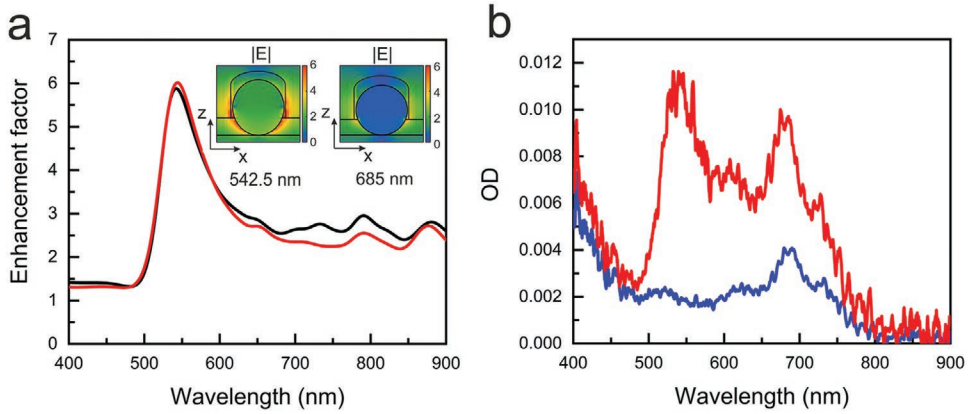

Figure 7. Coupled "fingerprint"-LSP absorption band promotes the internal optical transition of CT complexes. a) Absorption enhancement factor of ZnPc molecules in the hybrid AuNPs–ZnPc structure in the absence of NO_2 (black) and under NO_2 exposure (red). Inset – spatial distribution of E-field $|E|$ in the hybrid structure under NO_2 exposure, black lines represent contours of AuNP and ZnPc layers). b) Effective absorption spectrum of ZnPc in the hybrid structure (red) and the bare ZnPc monolayer (blue) under NO_2 exposure.

factor calculated for two cases: with NO_2 molecules attached and without it. It turns out NO_2 coordination to ZnPc molecules does not influence LSP mode distribution significantly, unlike the electronic configuration of molecular orbitals. Therefore, concentrated electric field of LSP mode boosts light absorption of $ZnPc^+$-NO_2^- complexes at the "fingerprint" band. Stemming on this result, we have calculated the effective absorption spectrum of CT complexes shown in Figure 7b. Apart from the great absorption enhancement by a factor of six, we would like to emphasize the qualitative difference in absorption of CT complexes modified by LSP modes comparing the initial one. Instead of strong maxima at 685 nm, it gives rise to the double peak spectrum with the main one located at 535 nm.

Last but not the least, we examined contribution of the redshift of LSP resonance into the overall "fingerprint"-LSP band. Since the marginal effect of NO_2 on the LSP mode distribution and its oscillator strength, we resume the redshift of about 2 nm plays a secondary role in the shape of differential spectra; it exclusively relates to the minimum at the asymmetric s-shaped resonance. Therefore, plasmon enhanced absorption of CT complexes is the main contribution to the "fingerprint"-LSP band and underlying mechanisms for the improved NO_2 gas sensing properties.

3. Conclusion

The developed fabrication technique is simple and can be easily scaled for different substrate areas and forms enabling creation of functional hybrid AuNP–ZnPc monolayer coatings with weak intermolecular interaction. The monomer-like character of the ZnPc monolayer should benefit overall photochemical activity of the structure by means of two aspects at least: 1) plasmon-enhanced absorption, 2) suppressed molecular aggregation. Our study reports substantial increase in absorption of the ZnPc monolayer promoted by LSP resonance; one can utilize it for various optoelectronic applications, particularly, in 2D semiconductor hybrid inorganic–organic heterostructures. The CT-complex formation has been shown under oxidation of ZnPc monolayer with NO_2 molecules in a gas phase. It results in the appearance of an unpaired electron at SOMO giving rise for the new band at 520 nm coupled to LSP resonance in hybrid AuNP–CT monolayer structure. We experimentally demonstrate the exciton–plasmon interaction greatly facilitating sensitivity of ZnPc monolayer to NO_2 gas detection by a factor of 15 at the mixed "fingerprint"-LSP absorption band which serves as the distinct feature of CT-complex formation. This principle can be straightforwardly extrapolated for the entire class of strong electron–donor/acceptor toxic analyte molecules like NO_2, NO, CO_2, CO, NH_3, and more, and even for lethal agents as dimethyl methylphosphonate (DMMP) and sarin.[57] We scrutinized light absorption mechanisms in the hybrid AuNP–CT monolayer and found out the sixfold increase in efficiency of the internal optical transition from nondegenerate low-lying doubly occupied orbitals toward degenerate half-empty orbital that can be exploited for ultrafast control over the SOMO–LUMO transition and possibly for switching an electronic configuration of SOMO via breaking its degeneracy. As there is only one electron at SOMO, a paramagnetic response from CT complexes can be anticipated. Therefore, the stable monomer-like ZnPc radical coupled to LSP resonance of gold particles is a promising system for further fundamental study of molecular magnetism with the prospect for organic spintronics. In the view of similarities in physicochemical properties of metal-substituted phthalocyanine compounds, we believe the developed principles can be easily extended to the entire family of phthalocyanines bearing different axial ligands with the promise for advanced and cost-effective metal-organic nanostructures with enhanced catalytic, sensing, optical, and magnetic properties.

4. Experimental Section

Materials: AuNPs of 2 nm diameter covered with dodecanethiol were purchased from PlasmaChem GmbH, Germany. Asymmetric ZnPc was synthesized according to the method described in ref. [41]. The structure of ZnPc and its UV–vis absorption spectra are presented in Figure S1, Supporting Information.

Langmuir–Blodgett (LB) Monolayer Preparation and Spectroscopy: A LB monolayer of AuNPs was prepared using KSV minithrough. A Wilhelmy plate was used for surface pressure control. Ultrapure water with a resistivity of ≈18 MΩ × cm was used as a subphase. The subphase temperature was regulated at 20 °C using a Julabo CD200F. 500 µL of AuNPs in chloroform (concentration of 1 mg mL^{-1}) was spread uniformly onto the subphase surface for isotherm measurements. After solvent evaporation (≈15 min), isotherm measurements were performed together with UV–vis spectroscopy of the monolayer. Absorption spectra were measured using a portable Ocean Optics HR4000 spectrometer, a fibre optical reflection/backscatter probe and a silver mirror, according to the method discussed in ref. [42]. Hydrophilic glass ($20 \times 20 \times (0.14 \div 0.17) mm^3$) was used as a substrate for monolayer transfer. Substrate purification was executed through boiling in methanol solution for 20 min. Then, in order to provide the hydrophilic surface of the substrate, it was boiled in a mixture of hydrogen peroxide and ammonia solution (volume ratio 1:1) for 10 min. All the prepared substrates were stored in ultrapure water (resistivity of ≈18 MΩ × cm) before the deposition procedure. The substrate was dipped in the subphase before the transfer process for Z-type film deposition. A 15 ± 0.3 mN m^{-1} surface pressure (surface pressure that corresponds to a linear region of the isotherm curve) and a barrier constant speed of 5 mm min^{-1} were maintained during monolayer deposition. The transfer speed was held constant (5 mm min^{-1}) and the transfer ratio was equal to 1 ± 0.3. After AuNPs deposition, sample was sintered at 230 °C during 1 h in order to desorb organic shell from nanoparticles.[43] The details on ZnPc monolayer transfer onto the substrates are described in Section S1b, Supporting Information.

Gas Testing Experiment: The sensing properties of the monolayers were tested using a purpose build setup, consisting of the gas chamber made of polytetrafluoroethylene and spectroscopy equipment (Ocean Optics HR 4000 spectrometer, HL-2000 light source, P600-2-UV–vis optical fibres and 74-UV collimating lenses). The optical transmittance of the samples was measured during the gas exposure. In the experiment, a mixture of nitrogen dioxide with pure nitrogen (N_2) with a concentration of 100 ppm, was used. The study of the recovery of the samples was carried out by heating to 60 °C using Peltier element.

Solution and Thin Film Spectroscopy: All solvents were of reagent-grade quality and were obtained directly from Aldrich. UV–vis spectroscopy of thin films deposited onto glass substrates was carried out using Ocean Optics HR400 spectrometer, HL-2000 light source, optical fibres (Ocean Optics P600-2-UV-VIS), and collimating lenses (Ocean Optics 74-UV).

Scanning Electron Microscopy (SEM): The morphology of the prepared samples was characterized by means of high-resolution field-emission scanning electron microscope (JEOL JSM-7200F). The SE (secondary electron) detector was used to analyze gold nanoparticles distribution at the hydrophilic glass surface.

FDTD Simulation: Theoretical verification of the enhanced absorption and gas sensing properties was made using FDTD simulation method.

In order to simplify calculations, the array of AuNPs with random distribution was replaced by periodic structure of AuNPs. Bloch boundary conditions were applied on the sides of the unit cell for simulation of an infinite array. Normally incident linearly polarized plane wave of 400–900 nm wavelengths was utilized for excitation.

Quantum-Chemical Calculations (DFT): Quantum chemical calculations were performed using density functional theory (DFT) and GAMESS-US Software[45] to optimize the structures of cation radical charge-transfer complexes of NO_2 with low-symmetry zinc phthalocyanine. The hybrid, 27% HF exchange, DFT meta-GGA M06 functional,[46] and 6–31+G* basis set were utilized for this purpose. The vibrational analysis was performed to confirm whether the optimized geometries correspond to local minima without imaginary frequencies. *Tert*-butyl substituents were replaced with hydrogen atoms to reduce the calculation time. A Linux/Intel cluster (www.jscc.ru) was used for the calculations.

Supporting Information

Supporting Information is available from the Wiley Online Library or from the author.

Acknowledgements

The authors would like to pay their gratitude and respects to Prof. Larisa G. Tomilova, who suddenly and unexpectedly passed away on the 4th of January 2021. The memory of her will forever remain in the hearts of all friends, colleagues, and students.

D.M.K. thanks D.O. Ignatyeva and A.N. Kalish for fruitful discussions on plasmon-assisted optical phenomena. The work was supported by the Russian Science Foundation (Grant No. 20-72-10145). A.Y.T. acknowledges the support by the State Assignment of 2020 (Theme 45.5 Creation of compounds with given physicochemical properties, No 0090-2019-0003) concerning the synthesis and quantum-chemical investigations of the phthalocyanine. V.E.P. acknowledges support by Council under the President of the Russian Federation for State Support of Young Scientists and Leading Scientific Schools (Grant MD-3847.2019.3). Authors thank the Joint Supercomputer Centre of RAS (www.jscc.ru) for providing computing resources.

Conflict of Interest

The authors declare no conflict of interest.

Data Availability Statement

All data supporting this study are openly available from the University of Southampton repository at https://doi.org/10.5258/SOTON/D1772.

Keywords

charge-transfer complexes, gas sensors, hybrid monolayers, internal optical transitions, resonant plasmon enhancement

Received: January 12, 2021
Revised: February 13, 2021
Published online:

[1] A. E. Braun, J. Tcherniac, *Eur. J. Inorg. Chem.* **1907**, *40*, 2709.
[2] S. Y. Chow, P. C. Lo, D. K. Ng, *Dalton Trans.* **2016**, *45*, 13021.
[3] M. Tanaka, in *High Performance Pigments*, 2nd edition (Eds: E. B. Faulkner, R. J. Schwartz), Wiley, New York, NY **2009**, Ch.17.
[4] F. Lv, X. He, L. Wu, T. Liu, *Bioorg. Med. Chem. Lett.* **2013**, *23*, 1878.
[5] D. Gounden, N. Nombona, W. E. van Zyl, *Coord. Chem. Rev.* **2020**, *420*, 213359.
[6] F. Baldini, A. Capobianchi, A. Falai, G. Pennesi, *Sens. Actuators, B* **1998**, *51*, 176.
[7] R. Zeis, T. Siegrist, C. Kloc, *Appl. Phys. Lett.* **2005**, *86*, 022103.
[8] I. Nar, A. Atsay, A. Altindal, E. Hamuryudan, *Inorg. Chem.* **2018**, *57*, 2199.
[9] K. Takanabe, K. Kamata, X. Wang, M. Antonietti, J. Kubota, K. Domen, *Phys. Chem. Chem. Phys.* **2010**, *12*, 13020.
[10] S. U. Khan, S. A. Trashin, Y. S. Korostei, T. V. Dubinina, L. G. Tomilova, S. W. Verbruggen, K. De Wael, *ChemPhotoChem* **2020**, *4*, 300.
[11] A. Satake, Y. Kobuke, *Org. Biomol. Chem.* **2007**, *5*, 1679.
[12] G. Bottari, O. Trukhina, M. Ince, T. Torres, *Coord. Chem. Rev.* **2012**, *256*, 2453.
[13] E. Coronado, *Nat. Rev. Mater.* **2020**, *5*, 87.
[14] M. Urdampilleta, S. Klayatskaya, M. Ruben, W. Wernsdorfer, *ACS Nano* **2015**, *9*, 4458.
[15] J. Schwöbel, Y. Fu, J. Brede, A. Dilullo, G. Hoffmann, S. Klyatskaya, M. Ruben, R. Wiesendanger, *Nat. Commun.* **2012**, *3*, 953.
[16] M. Warner, S. Din, I. S. Tupitsyn, G. W. Morley, A. M. Stoneham, J. A. Gardener, Z. Wu, A. J. Fisher, C. W. M. Kay, S. Heutz, G. Aeppli, *Nature* **2013**, *503*, 504.
[17] D. G. Lidzey, D. D. C. Bradley, M. S. Skolnick, T. Virgili, S. Walker, D. M. Whittaker, *Nature* **1998**, *395*, 53.
[18] R. Jayaprakash, K. Georgiou, H. Coulthard, A. Askitopoulos, S. K. Rajendran, D. M. Coles, A. J. Musser, J. Clark, I. D. W. Samuel, G. A. Turnbull, P. G. Lagoudakis, *Light: Sci. Appl.* **2019**, *8*, 81.
[19] J. Li, L. Gu, R. Wu, *Nanoscale* **2020**, *12*, 3888.
[20] S. Padgaonkar, S. H. Amsterdam, H. Bergeron, K. Su, T. J. Marks, M. C. Hersam, E. A. Weiss, *J. Phys. Chem. C* **2019**, *123*, 13337.
[21] J. Choi, H. Zhang, J. H. Choi, *ACS Nano* **2016**, *10*, 1671.
[22] N. Mutz, S. Park, T. Schultz, S. Sadofev, S. Dalgleish, L. Reissig, N. Koch, E. J. W. List-Kratochvil, S. Blumstengel, *J. Phys. Chem. C* **2020**, *124*, 2837.
[23] T. R. Kafle, B. Kattel, P. Yao, P. Zereshki, H. Zhao, W. L. Chan, *J. Am. Chem. Soc.* **2019**, *141*, 11328.
[24] A. V. Zasedatelev, T. V. Dubinina, D. M. Krichevsky, V. I. Krasovskii, V. Y. Gak, V. E. Pushkarev, L. G. Tomilova, A. A. Chistyakov, *J. Phys. Chem. C* **2016**, *120*, 1816.
[25] T. P. Mthethwa, S. Tuncel, M. Durmuş, T. Nyokong, *Dalton Trans.* **2013**, *42*, 4922.
[26] Y. Hu, J. Kanka, K. Liu, Y. Yang, H. Wang, H. Du, *RSC Adv.* **2016**, *6*, 104819.
[27] D. Steinebrunner, G. Schnurpfeil, A. Wichmann, D. Wöhrle, A. Wittstock, *Catalysts* **2019**, *9*, 555.
[28] P. Di Mascio, G. R. Martinez, S. Miyamoto, G. E. Ronsein, M. H. Medeiros, J. Cadet, *Chem. Rev.* **2019**, *119*, 2043.
[29] E. A. Kuzmina, T. V. Dubinina, A. V. Zasedatelev, A. V. Baranikov, M. I. Makedonskaya, T. B. Egorova, L. G. Tomilova, *Polyhedron* **2017**, *135*, 41.
[30] N. Nwaji, J. Mack, T. Nyokong, *Opt. Mater.* **2018**, *82*, 93.
[31] O. M. Bankole, O. Osifeko, T. Nyokong, *J. Photochem. Photobiol., A* **2016**, *329*, 155.
[32] N. Nwaji, B. Jones, J. Mack, D. O. Oluwole, T. Nyokong, *J. Photochem. Photobiol., A* **2017**, *346*, 46.
[33] N. C. Jeong, C. Prasittichai, J. T. Hupp, *Langmuir* **2011**, *27*, 14609.
[34] T. Akiyama, M. Nakada, N. Terasaki, S. Yamada, *Chem. Commun.* **2006**, 395.
[35] T. Kawawaki, Y. Takahashi, T. Tatsuma, *J. Phys. Chem. C.* **2013**, *117*, 5901.
[36] T. Ming, L. Zhao, Z. Yang, H. Chen, L. Sun, J. Wang, C. Yan, *Nano Lett.* **2009**, *9*, 3896.
[37] W. Zhang, H. Lei, *Nanoscale* **2020**, *12*, 6596.

[38] M. Wang, B. Bangalore Rajeeva, L. Scarabelli, E. P. Perillo, A. K. Dunn, L. M. Liz-Marzán, Y. Zheng, *J. Phys. Chem. C* **2016**, *120*, 14820.
[39] F. Le, D. W. Brandl, Y. A. Urzhumov, H. Wang, J. Kundu, N. J. Halas, J. Aizpurua, P. Nordlander, *ACS Nano* **2008**, *2*, 707.
[40] C. L. Haynes, R. P. Van Duyne, *J. Phys. Chem. B* **2003**, *107*, 7426.
[41] A. Y. Tolbin, V. E. Pushkarev, G. F. Nikitin, L. G. Tomilova, *Tetrahedron Lett.* **2009**, *50*, 4848.
[42] J. J. Burack, J. D. LeGrange, J. L. Markham, W. Rockward, *Langmuir* **1992**, *8*, 613.
[43] B. L. Smith, J. E. Hutchison, *J. Phys. Chem. C* **2013**, *117*, 25127.
[44] D. M. Krichevsky, A. V. Zasedatelev, A. Y. Tolbin, S. Y. Luchkin, A. B. Karpo, V. I. Krasovskii, L. G. Tomilova, *Thin Solid Films* **2017**, *642*, 295.
[45] M. W. Schmidt, K. K. Baldridge, J. A. Boatz, S. T. Elbert, M. S. Gordon, J. H. Jensen, S. Koseki, N. Matsunaga, K. A. Nguyen, S. Su, T. L. Windus, M. Dupuis, J. A. Montgomery, *J. Comput. Chem.* **1993**, *14*, 1347.
[46] Y. Zhao, D. G. Truhlar, *Theor. Chem. Acc.* **2008**, *120*, 215.
[47] H. AlQahtani, M. Sugden, D. Puzzovio, L. Hague, N. Mullin, T. Richardson, M. Grell, *Sens. Actuators, B* **2011**, *160*, 399.
[48] R. R. Abbas, T. H. Richardson, A. Hobson, A. Hassan, T. R. Abbas, *Colloids Surf. A* **2014**, *444*, 95.
[49] D. E. Nevonen, G. T. Rohde, V. N. Nemykin, *Inorg. Chem.* **2019**, *58*, 14120.
[50] T. Nyokong, Z. Gasyna, M. J. Stillman, *Inorg. Chem.* **1987**, *26*, 548.
[51] T. Nyokong, Z. Gasyna, M. J. Stillman, *Inorg. Chem.* **1987**, *26*, 1087.
[52] J. Šebera, P. Fitl, J. Vlček, M. Vrňata, F. Fendrych, J. Kopeček, I. Kratochvílová, *Eur. Phys. J. Appl. Phys.* **2013**, *64*, 10202.
[53] M. Chaabene, B. Gassoumi, P. Mignon, R. B. Chaâbane, A. R. Allouche, *J. Mol. Graphics Modell.* **2019**, *88*, 174.
[54] L. S. Chia, Y. H. Du, S. Palale, P. S. Lee, *ACS Omega* **2019**, *4*, 10388.
[55] D. M. Krichevsky, A. V. Zasedatelev, A. Y. Tolbin, Y. M. Zelenskiy, V. I. Krasovskii, A. B. Karpo, L. G. Tomilova, *J. Phys.: Conf. Ser.* **2016**, *737*, 012030.
[56] A. V. Zasedatelev, D. M. Krichevsky, Y. M. Zelenskiy, A. Y. Tolbin, V. I. Krasovskii, A. B. Karpo, L. G. Tomilova, *J. Phys.: Conf. Ser.* **2016**, *737*, 012031.
[57] H. Aldahhak, P. Powroznik, P. Pander, W. Jakubik, F. B. Dias, W. G. Schmidt, M. Krzywiecki, *J. Phys. Chem. C* **2020**, *124*, 6090.